Research article

Sicong Liu, Yonggang Wang*, Ruidong Lv, Jiang Wang, Huizhong Wang, Yun Wang and Lina Duan

2D molybdenum carbide (Mo_2C)/fluorine mica (FM) saturable absorber for passively mode-locked erbium-doped all-fiber laser

https://doi.org/10.1515/nanoph-2020-0019
Received January 12, 2020; revised February 15, 2020; accepted February 16, 2020

Abstract: As a new member of saturable absorber (SA), molybdenum carbide (Mo_2C) has some excellent optical properties. Herein, we report a new type of Mo_2C/fluorine mica (FM) SA device. Uniform and compact Mo_2C films were deposited on the FM by magnetron sputtering method. In order to increase the laser damage threshold, an additional protective layer of silicon oxide was deposited on the Mo_2C. The FM is a single-layer structure of 20 μm, and its high elasticity makes it not easy to fracture. The transmission rate of FM is as high as 90% at near infrared wavelength. FM has better heat dissipation and softening temperature than organic composite materials, so it can withstand higher laser power without being damaged. In this work, Mo_2C/FM SA was cut into small pieces and inserted into erbium-doped fiber laser to achieve mode-locked operation. The pulse duration and average output power of the laser pulses were 313 fs and 64.74 mW, respectively. In addition, a 12th-order sub-picosecond harmonic mode-locking was generated. The maximum repetition rate was 321.6 MHz and the shortest pulse duration was 338 fs. The experimental results show that Mo_2C/FM SA is a broadband nonlinear optical mode-locker with excellent performance.

***Corresponding author: Yonggang Wang,** School of Physics and Information Technology, Shaanxi Normal University, Xi'an 710119, China; and State Key Laboratory of Transient Optics and Photonics, Xi'an Institute of Optics and Precision Mechanics, Chinese Academy of Sciences, Xi'an 710119, China, e-mail: chinawygxjw@snnu.edu.cn
Sicong Liu, Ruidong Lv, Jiang Wang, Huizhong Wang and Yun Wang: School of Physics and Information Technology, Shaanxi Normal University, Xi'an 710119, China.
https://orcid.org/0000-0002-7507-4106 (S. Liu)
Lina Duan: School of Science, Xi'an Shiyou University, Xi'an 710065, China

Keywords: molybdenum carbide; mode-locking laser; magnetron-sputtering deposition (MSD) method.

1 Introduction

As an important branch of modern optics, nonlinear optics mainly studies the optical nonlinear phenomenon and its application. Nonlinear optics is of great significance in the development of laser technology, spectroscopy, and material structure analysis [1, 2]. The emergence of laser characterized by a high degree monochromaticity, high intensity, and high directionality has also made nonlinear optics one of the fastest-growing scientific fields in recent decades [3, 4]. Nonlinear optical processing is closely related to the development of ultrashort pulse laser technology [5, 6]. Among them, saturable absorption plays a key role as a nonlinear optical phenomenon to obtaining ultrashort pulses. The range of time resolved measurements is therefore extended to femtoseconds [7, 8].

One of the effective technologies to realize ultrashort pulse is mode-locking technology based on saturable absorbers (SAs) [9–13]. SAs rely on the nonlinear optical response of a saturated absorbing material. The optical absorption of the SA decreases with the increase in incident light intensity [14, 15]. The ultrashort laser pulses with high peak power can be generated by mode-locking or Q-switching, depending on the nonlinear optical response of the SA [16]. SA-based fiber lasers have the advantages of compact structure, good mechanical stability, high reliability, good beam quality, high scalability, easy implementation, and low cost [17, 18]. In recent years, fiber lasers have been widely used in industrial laser micromachining [19], ultrafast information processing [20], and molecular spectroscopy [21]. Until now, the commercial semiconductor saturable absorption mirror still has some defects, such as limited working bandwidth, expensive fabrication cost and, complex process. Therefore, people have been

concerned about the saturated absorption characteristics of low dimensional nanomaterials, in order to develop a broadband SA with high performance and high cost performance for ultrashort pulse.

For this reason, many kinds of materials have been studied, such as graphene [22–24], transition metal dichalcogenides (e.g. MoS_2, WS_2) [25–27], black phosphorus [28–31], carbon nanotubes [32, 33], topological insulators (TIs) [34, 35], perovskite [36–38], and other nonlinear materials [39–42], which proves that these materials have good saturated absorption properties or application prospects. However, the development of nonlinear optical properties of new materials still has far-reaching significance.

In recent years, Mxenes, as a new class of two-dimensional (2D) materials, has attracted great interest among researchers in the development of new ultrafast photonics applications. As one of Mxenes, transition metal carbides (TMCs) have been proven to have excellent physical and chemical properties, such as high hardness, high melting point, and high stability, which can be used in energy storage and catalysis [43–47]. The band structure and electronic density of state of 2D TMCs have been studied extensively by using the density functional theory method [48]. The 2D TMCs have ultrahigh conductivity, similar to graphene, because of the incorporation of carbon atoms into the metal lattice and are normally metallic with a high electron density near the Fermi level [12, 49]. Considering the recent progress on the synthesis of large size and highly crystalline Mo_2C [47], it is nontrivial to integrate such material onto optical fiber with improved fabrication approach and further explore the nonlinear absorption properties as well as the application for ultrafast lasers. In 2018, Tuo et al. reported mode-locked erbium (Er)-doped or Yb-doped fiber lasers, using the Mo_2C nanocrystal as an SA [50]. It was been proved that Mo_2C has the advantages of excellent saturable absorption properties, low saturation intensity, and tunable modulation depth (MD). However, the pulse width of the laser is too wide and the power is low. Therefore, it is necessary to explore more possibility of Mo_2C material in mode-locked laser.

In this paper, Mo_2C films were prepared by magnetron sputtering method (MSD) with fluorine mica (FM) sheet as the substrate and the quality of the films was examined by material characterization. Furthermore, the potential of Mo_2C thin films to produce mode-locked laser pulses was explored in the fiber laser. In order to further improve the damage threshold of SA and effectively avoid material oxidation and falling off, silicon oxide (SiO_2) was sputtered on Mo_2C film as a protective layer. A very stable femtosecond mode-locked soliton pulse is obtained by inserting Mo_2C/FM into Er-doped fiber laser. In addition, high repetition frequency harmonic mode-locking (HML) is also generated by adjusting the polarization controller and pump power. The experimental results show that Mo_2C/FM has good nonlinear absorption characteristics and can be used to realize fundamental soliton and high frequency harmonic femtosecond pulse laser.

2 Fabrication and characterization of Mo_2C

In order to prepare high-performance Mo_2C SA, we selected monolayer FM as the substrate of the material. FM is a kind of material with good light transmittance and high intensity laser resistance. The SA device based on FM can resist strong laser damage and achieve high modulation ability. First, concentrated sulfuric acid and concentrated hydrochloric acid are used for hydrophilic treatment of mica to enhance the adhesion of the film on the mica surface. The mica sheet was washed repeatedly by alcohol and deionized water, and then the treated mica sheet was dried in a drying oven at 40°C. The FM and Mo_2C target with a purity of 99.99% are put into a sputtering chamber of a magnetron sputtering system. The vacuum of the chamber is pumped to a vacuum degree of 6.8×10^{-4} pa by a mechanical pump and a molecular pump. In order to ensure the uniformity of the formation of the Mo_2C film, the FM was rotated at a speed of 30 r/min. The Mo_2C/FM films were placed in the super clean box after sputtering. The Mo_2C target was removed and chamber was washed repeatedly with acetone, alcohol, and other reagents. After that, the SiO_2 target with purity of 99.99% is mounted, and the Mo_2C/FM prepared before is sputtered under the same vacuum, pressure, power, and rotation speed for 1 min. Finally, the Mo_2C/FM SA for mode locked fiber laser was obtained. Thereafter, the Mo_2C films were characterized by Raman spectrum, transmission electron microscopy (TEM), atomic force microscope (AFM), and scanning electron microscopy (SEM). We measured the Raman spectrum of the Mo_2C material by using a 532-nm laser. As shown in Figure 1A, there are two typical peaks, which are located at 1351^{-1} cm and 1593^{-1} cm, respectively, corresponding to the D and G bands of carbon. The D peak usually indicates the vibration of the SP^3 hybridized carbon atom, which represents amorphous carbon and disordered carbon. And the G peak can represent the degree of graphitization, which is related to the existence of the SP^2 carbon structure. Figure 1B shows a low- and

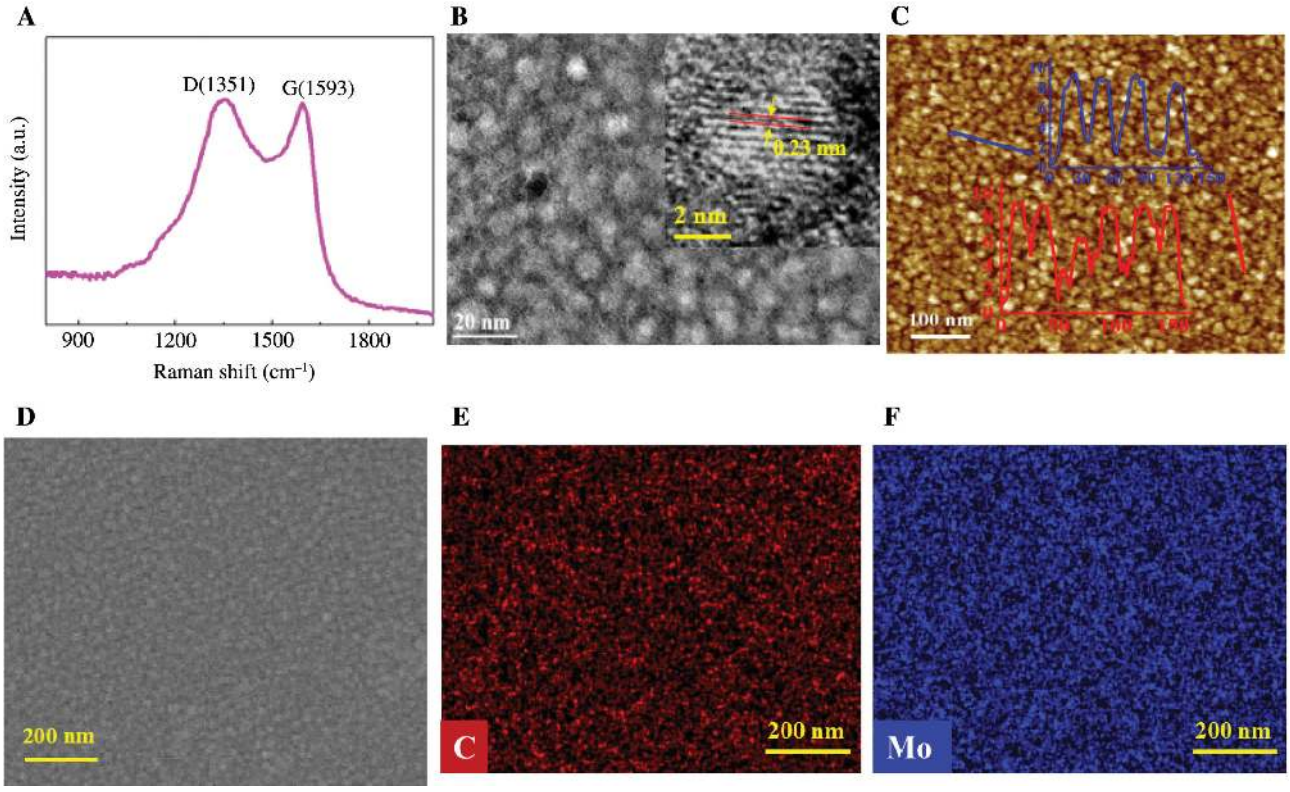

Figure 1: Characterization of Mo_2C film.
(A) Raman spectrum. (B) Low- and high-magnification HRTEM images of Mo_2C materials. (C) AFM images and height profiles showing the thickness of the 2D Mo_2C film. (D) SEM images of the Mo_2C. (E, F) element mapping of C and Mo.

high-magnification high-resolution TEM (HRTEM) image of the Mo_2C materials. The inset is an image showing lattice fringes with an interplanar spacing of 0.23 nm corresponding to the Mo_2C (101) planes. In addition, the thickness of the prepared Mo_2C film sample was approximately 9 nm as seen from the AFM image and the height profile of Figure 1C. The field emission SEM image of Mo_2C film is shown in Figure 1D. It can be seen from the figure that the Mo_2C film has excellent surface uniformity. Figure 1E and F show the element mapping of Mo_2C, which is detected to contain molybdenum and carbon.

In addition, in order to obtain the optical properties of the Mo_2C/FM SA, ultraviolet-visible-infrared supercontinuous light sources are used to measure the transmittance. The measurement range is 1000–2000 nm, as shown in Figure 2A. At the 1550 nm wavelength, the transmittance of SA is about 75.68%. The open aperture Z-scan measurements were employed to investigate the nonlinear optical

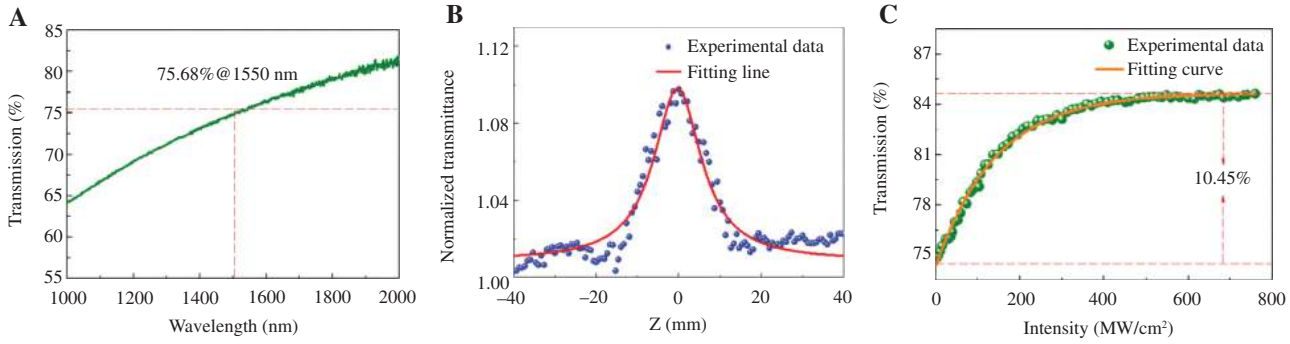

Figure 2: Transmittance of Mo_2C.
(A) Measured linear transmittance of Mo_2C material. (B) The position-dependent nonlinear transmittance of the Mo_2C film measured by Z-scan method. (C) Nonlinear transmission of Mo_2C/FM SA.

response of Mo_2C film with a wavelength of 1550 nm. As shown in Figure 2B, the normalized transmittance gradually increased when the Mo_2C thin film drew near to the focus of the beam, indicating that the absorption of Mo_2C became saturated with the increase in the incident pump intensity. Finally, the nonlinear optical absorption characteristics of SA were measured by a self-made mode-locked fiber laser with a center wavelength of 1550 nm (pulse width of 600 fs and fundamental frequency of 32 MHz). The laser is divided into two beams by the 50:50 coupler, and the two beams are used for power-dependent transmission measurement of SA and for reference, respectively. The measured results are fitted by the function $T = 1 - \Delta T^* \exp(-I/I_{sat}) - T_{ns}$. Here, T is the transmission rate, I is the incident intensity, ΔT is the MD, I_{sat} is the saturation intensity, and T_{ns} is the non-saturable loss (NL). The nonlinear saturated absorption curve is shown in Figure 2C, in which the MD, NL, and I_{sat} are 10.45%, 15.3%, and 143.3 MW/cm^2, respectively. It can be seen that Mo_2C/FM SA exhibits significant nonlinear properties.

3 Experimental setup of the fiber laser

We constructed an all-fiber Er-doped fiber laser to research the optical performance of the Mo_2C/FM SA device. The experimental schematic diagram of the mode-locked fiber laser is shown in Figure 3. The total ring cavity length of the fiber laser was 7.6 m. It contained 0.5 m Er-doped gain fiber with a group velocity dispersion of –10.55 ps/(nm · km) and 7.1 m standard single mode fiber (SMF28) with a group velocity dispersion of 17 ps/(nm · km) at communication band (C-band). Therefore, the amount of net dispersion in the cavity was probably

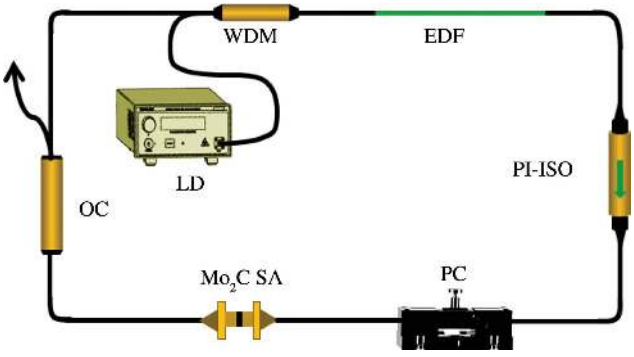

Figure 3: Schematic diagram of passively mode-locked erbium-doped fiber (EDF) laser system.

–0.147 ps^2. A wavelength of 976 nm laser diode with a maximum output power of 700 mW was transmitted through a 980/1550 nm wavelength division multiplexer coupler. In order to ensure that the laser transmits unidirectionally in the ring cavity, a polarization independent isolator was employed in the cavity. By adjusting the polarization controller (PC) to change the birefringence of the fiber, the polarization state of the laser in the cavity can be adjusted. A 50:50 optical fiber coupler was used for output the laser emission. The Mo_2C/FM was sandwiched between the two fiber ferrules. By adjusting the pump power and PC, mode-locking operation was realized. The optical spectrum analyzer (Yokogawa AQ6370D) and a radiofrequency (RF) analyzer (Rohde & Schwarz FSV 13) were used to monitor and collect data in the frequency domain. In the time domain, a 1G digital oscilloscope (ROHDE & SCHWARZRTO1014) with a home-made 5G photodetector requipped and an optical autocorrelator (APE Pulse check) were used to monitor and measure the pulse sequence.

4 Results and discussion

4.1 Mode-locking

In this experiment, self-started soliton mode-locking was obtained by increasing the pump power and adjusting the polarization state using PC. The optical spectrum of mode-locked laser was observed at 1558.03 nm and 3-dB spectral width is 13.75 nm as shown in Figure 4A. Figure 4B shows the auto-correlation trace of the soliton mode-locked fiber laser. The measured autocorrelation trace of the pulse is fitted with the Sech^2 function, and the pulse duration is estimated to be 313 fs. The time-bandwidth product is 0.532, which is larger than the transformation limit of Fourier transform. This implied that the mode-locked pulses have chirp. The time trace of oscilloscope is shown in Figure 4C, the 37.3 ns pulse interval corresponds to the total cavity length of 7.6 m. The frequency spectrum of the output pulse is measured in order to further monitor the stability of the mode-locking laser. The signal-to-noise ratio (SNR) of the fundamental frequency was shown to be 79 dB, as shown in Figure 4D. Furthermore, the dependence between the output power of the mode-locked and the pump power is measured as shown Figure 4E. The output power increased linearly to 64.74 mW and the slope efficiency is 10% when the pump power is increased to 700 mW. During the experiment, the mode-locking operation was always stable when the

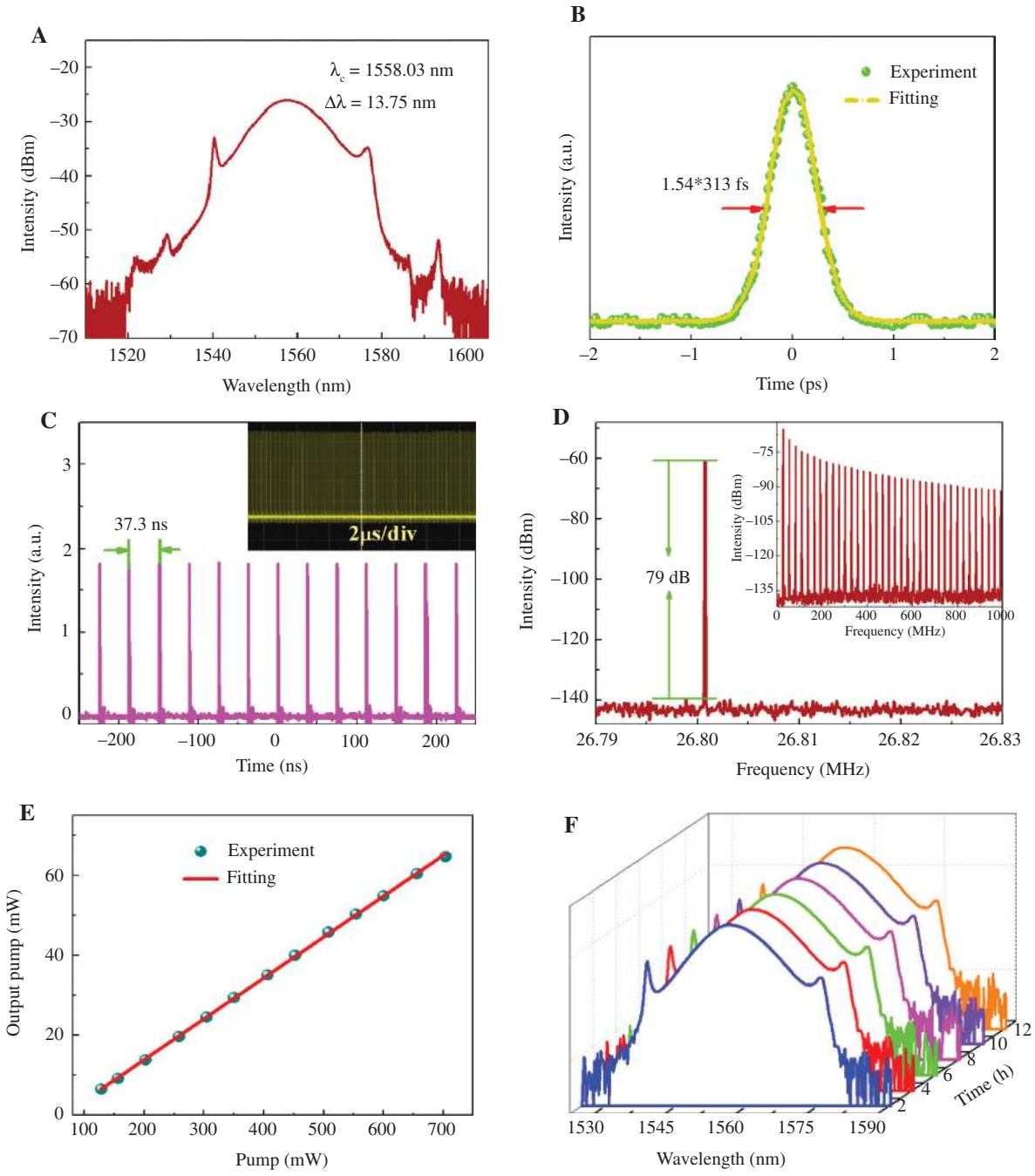

Figure 4: Typical mode-locked fiber laser characteristics.
(A) Typical mode-locked optical spectrum. (B) The corresponding autocorrelation trace. (C) Pulse trains of oscilloscope. (D) Radiofrequency spectrum. (E) Relationship between output power and pump power. (F) The output spectra measured every 2 h showing long-term stability of the mode-locking state.

pump power was gradually increased from the self-start threshold (100 mW) to the pump maximum output power (700 mW). If the pump power is further increased, the output power can be increased again. However, due to the limitation of the maximum power of the pump source, the output power cannot be further improved. The results indicate that the Mo_2C/FM SA has the advantage of a high optical damage threshold. To further illustrate the stability of the mode-locking, the laser is continuously operated for 12 h without interruption. The spectra were recorded every 2 h, as shown in Figure 4F. It can be found that the spectrum does not degrade during the test time. In Table 1,

Table 1: Output performance comparison of 1.55 μm mode-locked fiber lasers using various 2D-material-based SAs.

Materials	SA type	MD	NL	λ	τ(fs)	Average power	Ref.
MoS_2	Langmuir-Blodgett	5.9	13.4	1557	581	9.6 mW	[9]
Graphene	Chemical vapor deposition	6.2–66.5	–	1565	756	40 mW	[22]
WSe_2	Polymethyl methacrylate-Microfiber	54.5	–	1556	477	–	[27]
WS_2	Taper	0.5	65.0	1563	563	2.8 mW	[26]
BP	Mechanical exfoliation	8.1	–	1571	946	–	[29]
TI	Polyol method	98		1564	1570	–	[35]
Perovskite	Precursor solutions	27.8	–	1555	661	–	[38]
Mo_2C	FM-MSD film	10.45	15.3	1558	313	64.74 mW	Our work

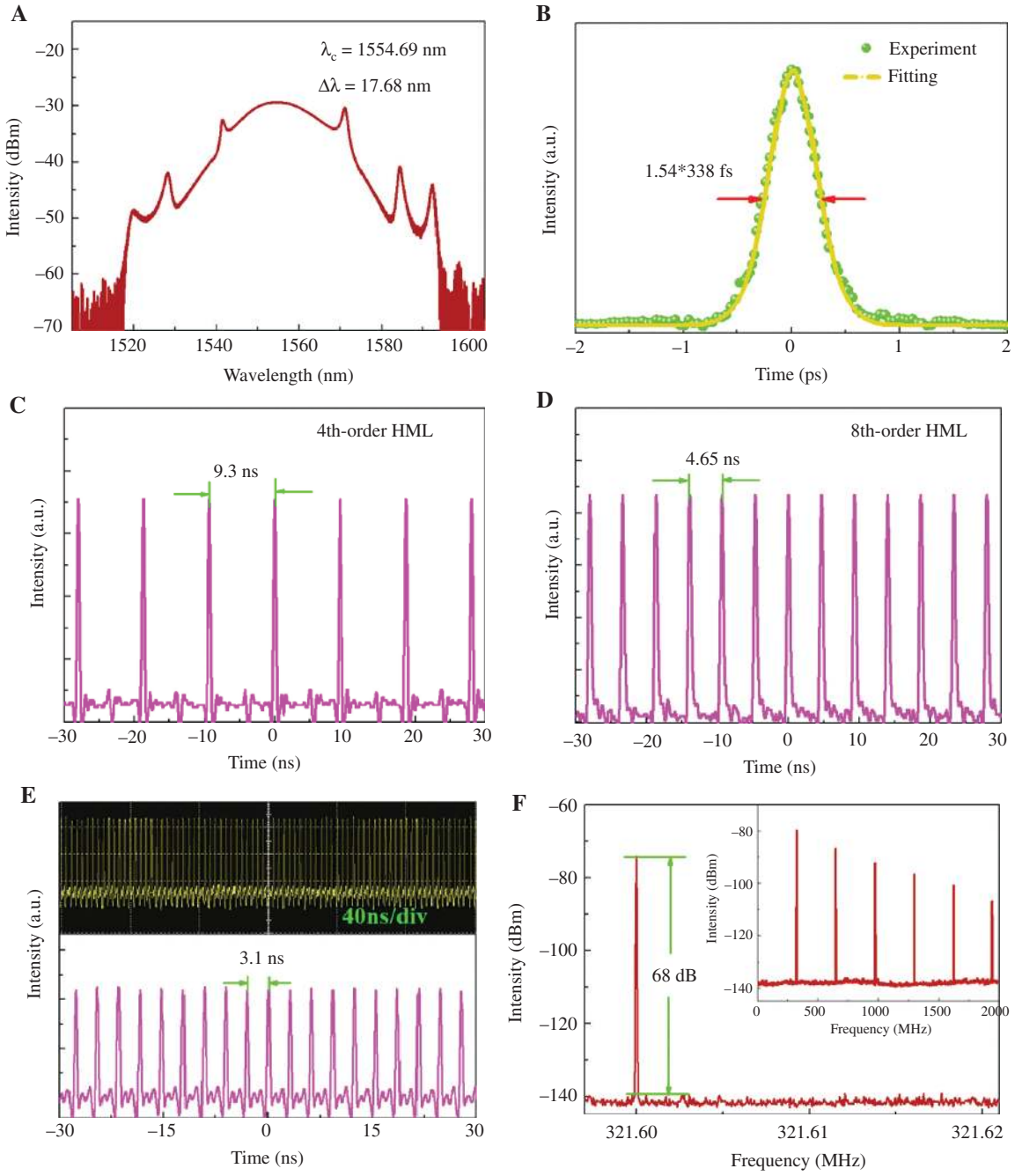

Figure 5: Typical mode-locking pulse output characteristics.
(A) Optical spectra. (B) Autocorrelation traces. (C–E) Oscilloscope trace of the 4th HML, 8th HML, and 12th HML. (F) RF spectra.

we compared the nonlinear parameters of typical SAs and corresponding laser properties. The MD of Mo_2C/FM SA is lower than that of graphene and Ti, but higher than that of most other SAs. It is important that the pulse width and output power of Mo_2C/FM SA are much better than those of other SA lasers, suggesting that Mo_2C/FM SA has excellent ultrafast photonics properties.

In order to verify the cause of the mode-locking operation, we intentionally removed the SA from the laser cavity. Mode-locking cannot be observed any longer by adjusting the PC and pump power over a wide range. However, the mode-locking operation can be realized again as soon as the Mo_2C/FM SA was inserted into the laser cavity. Therefore, it can be inferred that the mode-locking operation is caused by the SA rather than other components.

4.2 Harmonic mode-locking

In the same fiber laser cavity, HML can be obtained by increasing pump power and adjusting the PC. After that, as the pump power is gradually increased, different orders of HML states can be obtained. In this experiment, the highest pulse repetition rate of HML that can be measured is 321.6 MHz, which corresponds to the 12th harmonic of fundamental repetition frequency. As shown in Figure 5A, the 3-dB bandwidth of the harmonic mode-locked spectrum is 17.68 nm, and the central wavelength is 1554.69 nm. Figure 5B shows the auto-correlation trace of the 12th HML output with a full width half maximum of 520 fs. The trace is fitted by a $Sech^2$ function and the estimated pulse duration is 338 fs. By changing the power and adjusting the polarization state slightly, the laser can realize the continuous tunable frequency output from the 2nd harmonic to the 12th harmonic. The pulse sequences of the 4th, 8th, and 12th harmonic detected by the oscilloscope are shown in Figure 5C–E, the pulse has relatively uniform intensity and time interval. The RF spectrum in Figure 5F shows that the SNR determined by the pulse sequence is 68 dB. The fundamental peak was located at 321.6 MHz (pump power = 700 mW), which corresponds to the 12th HML state. At this time, the maximum average output power is 68.01 mW. In summary, it can be determined that the fiber laser at this time is operating in HML state. If a higher output power pump power is used, a higher order than the 12th HML state may be output. This provides many possibilities for the application of Mo_2C SA mode-locked laser, which can be used as potential light source for optical frequency comb and optical imaging.

5 Conclusions

To sum up, we prepared homogeneous and dense Mo_2C film on FM substrate by MSD technology. The surface morphology and nonlinear optical properties were studied. Mo_2C/FM film has the advantages of uniform surface distribution, small NL value, and high damage threshold. Mo_2C/FM SA is embedded in an Er-doped fiber laser with a ring cavity structure, which achieves stable fundamental mode-locking and high repetition frequency HML, respectively. For soliton mode-locked pulse, the output power and the pulse duration are 64.74 mW/313 fs at 1.5 μm regime, respectively. The maximum output power and the maximum repetition rate of the 12th harmonic mode locking are 68.01 mW and 321.6 MHz, respectively. Our experimental results show that Mo_2C/FM film has great practical value in ultrafast photonics and optoelectronics.

Acknowledgments: This work is supported by the Fundamental Research Funds for the Central Universities (2019TS117).

Conflicts of interest: There are no conflicts of interest to declare.

References

[1] Bloembergen N. Nonlinear optics and spectroscopy. Rev Mod Phys 1982;216:1057.
[2] He GS, Liu SH. Physics of nonlinear optics[M]. Singapore, World Scientific Publishing Co. Pte. Ltd., 1999.
[3] Brabec T, Krausz F. Intense few-cycle laser fields: frontiers of nonlinear optics. Rev Mod Phys 2000;72:545–91.
[4] Boyd RW. Nonlinear optics. Cambridge, MA: Academic Press, 2008.
[5] Steinmeyer G. Frontiers in ultrashort pulse generation: pushing the limits in linear and nonlinear optics. Science 1999;286:1507–12.
[6] Heatley DR, Firth WJ, Ironside CN. Ultrashort-pulse generation using two-photon gain. Opt Lett 1993;18:628.
[7] Haus H. Theory of mode locking with a slow saturable absorber. IEEE J Quantum Electron 1975;11:736–46.
[8] Letokhov VS. Generation of ultrashort light pulses in a laser with a nonlinear absorber. J Exp Theoretical Phys 1969;28:562.
[9] Lv RD, Wang YG, Wang J, et al. Soliton and bound-state soliton mode-locked fiber laser based on a MoS_2/fluorine mica Langmuir-Blodgett film saturable absorber. Photonics Res 2019;7:431–6.
[10] Chen Y, Jiang G, Chen S. Mechanically exfoliated black phosphorus as a new saturable absorber for both Q-switching and Mode-locking laser operation. Opt Express 2015;23:12823–33.

[11] Guo S, Zhang Y, Ge Y, et al. 2D V-V binary materials: status and challenges. Adv Mater 2019;31:1902352.
[12] Jiang XT, Liu SX, Liang WY, et al. Broadband nonlinear photonics in few-layer MXene Ti_3C_2Tx (T=F, O, or OH). Laser Photonics Rev 2018;12:1870013.
[13] Jhon YI, Lee J, Seo M, et al. Van der Waals layered tin selenide as highly nonlinear ultrafast saturable absorber. Adv Opt Mater 2019;7:1801745.
[14] Zhang H, Stéphane V, Bao Q, et al. Z-scan measurement of the nonlinear refractive index of graphene. Opt Lett 2012;37:1856.
[15] Xing G, Guo H, Zhang X, et al. The physics of ultrafast saturable absorption in graphene. Opt Express 2010;18:4564–73.
[16] Chernysheva M, Rozhin A, Fedotov Y, et al. Carbon nanotubes for ultrafast fibre lasers. Nanophotonics 2017;6:1–30.
[17] Keller U. Recent developments in compact ultrafast lasers. Nature 2003;424:831–8.
[18] Song YF, Shi XJ, Wu CF, et al. Recent progress of study on optical solitons in fiber lasers. Appl Phys Rev 2019;6:021313.
[19] Gattass RR, Mazur E. Femtosecond laser micromachining in transparent materials. Photonics 2008;2:219.
[20] Vivie-Riedle RD, Troppmann U. Femtosecond lasers for quantum information technology. Chem Rev 2007;107:5082–100.
[21] Diddams SA, Hollberg L, Mbele V. Molecular fingerprinting with the resolved modes of a femtosecond laser frequency comb. Nature 2007;445:627.
[22] Bao Q, Zhang H, Wang Y, et al. Atomic-layer graphene as a saturable absorber for ultrafast pulsed lasers. Adv Funct Mater. 2009;19:3077–83.
[23] Sun Z, Hasan T, Torrisi F, et al. Graphene mode-locked ultrafast laser. ACS Nano 2010;4:803–10.
[24] Peng KJ, Wu CL, Lin YH, et al. Saturated evanescent-wave absorption of few-layer graphene-covered side-polished single-mode fiber for all-optical switching. Nanophotonics 2017;7:207–15.
[25] Lv RD, Chen ZD, Liu SC, et al. Optical properties and applications of molybdenum disulfide/SiO_2 saturable absorber fabricated by sol-gel technique. Opt Express 2019;27:6348–56.
[26] Khazaeinezhad R, Kassani SH, Jeong H, et al. Ultrafast pulsed all-fiber laser based on tapered fiber enclosed by few-layer WS_2 nano-sheets. IEEE Photonics Technol Lett 2015;27:1581–4.
[27] Yin JD, Li JR, Chen H, et al. Large-area highly crystalline WSe_2 atomic layers for ultrafast pulsed lasers. Opt Express 2017;25:30020–31.
[28] Lu SB, Miao LL, Guo ZN, et al. Broadband nonlinear optical response in multi-layer black phosphorus: an emerging infrared and mid-infrared optical material. Opt Express 2015;23:11183.
[29] Chen Y, Jiang GB, Chen SQ, et al. Mechanically exfoliated black phosphorus as a new saturable absorber for both Q-switching and mode-locking laser operation. Opt Express 2015;23:12823–33.
[30] Guo Z, Zhang H, Lu S, et al. From black phosphorus to phosphorene: basic solvent exfoliation, evolution of Raman scattering, and applications to ultrafast photonics. Adv Funct Mater 2015;25:6996–7002.
[31] Xu YH, Wang ZT, Guo ZN, et al. Solvothermal synthesis and ultrafast photonics of black phosphorus quantum dots. Adv Opt Mater 2016;4:1223–9.
[32] Song YW, Yamashita S, Goh CS, et al. Carbon nanotube mode lockers with enhanced nonlinearity via evanescent field interaction in D-shaped fibers. Opt Lett 2007;2:148.
[33] Chernysheva MA, Krylov AA, Kryukov PG, et al. Thulium-doped mode-locked all-fiber laser based on NALM and carbon nanotube saturable absorber. Opt Express 2012;20:B124–30.
[34] Jhon YI, Lee J, Jhon YM, et al. Topological insulators for mode-locking of 2-μm fiber lasers. IEEE J Sel Top Quantum Electron 2018;24:1102208.
[35] Zhao C, Zou Y, Chen Y, et al. Wavelength-tunable picosecond soliton fiber laser with Topological Insulator: Bi_2Se_3 as a mode locker. Opt Express 2012;20:27888.
[36] Zhang Y, Lim CK, Dai Z, et al. Photonics and optoelectronics using nano-structured hybrid perovskite media and their optical cavities. Phys Rep 2019;795:1.
[37] Li PF, Chen Y, Yang TS, et al. Two-dimensional $CH_3NH_3PbI_3$ perovskite nanosheets for ultrafast pulsed fiber lasers. ACS Appl Mater Interfaces 2017;9:12759.
[38] Jiang GB, Miao LL, Yi G, et al. Ultrafast pulse generation from erbium-doped fiber laser modulated by hybrid organic–inorganic halide perovskites. Appl Phys Lett 2017;110:16111.
[39] Xie ZJ, Zhang F, Liang ZM, et al. Revealing of the ultrafast third-order nonlinear optical response and enabled photonic application in two-dimensional tin sulfide. Photonics Res 2019;7:494–502.
[40] Wu L, Xie Z, Lu L, et al. Few-layer tin sulfide: a promising black-phosphorus-analogue 2D material with exceptionally large nonlinear optical response, high stability, and applications in all-optical switching and wavelength conversion. Adv Opt Mater 2018;6:1700985.
[41] Xing C, Xie Z, Liang Z, et al. 2D nonlayered selenium nanosheets: facile synthesis, photoluminescence, and ultrafast photonics. Adv Opt Mater 2017;5:1700884.
[42] Huang WC, Xie ZJ, Fan TJ, et al. Black-phosphorus-analogue tin monosulfide: an emerging optoelectronic two-dimensional material for high-performance photodetection with improved stability under ambient/harsh conditions. J Mater Chem C 2018;6:9582–93.
[43] Zuo Y, Gao YR, Qin SY. Broadband multi-wavelength optical sensing based on photothermal effect of 2D MXene films. Nanophotonics 2019;9:123–31.
[44] Shi XR, Wang JG, Hermann K. CO and NO adsorption and dissociation at the β-Mo_2C(0001) surface: a density functional theory study. J Phys Chem C 2010;114:13630–41.
[45] Alexander M, Hargreaves JSJ. Alternative catalytic materials: carbides, nitrides, phosphides and amorphous boron alloys. Chem Soc Rev 2010;39:388–4401.
[46] Yang C, Zhao HB, Hou YL, et al. Fe_5C_2 Nanoparticles: a facile bromide-induced synthesis and as an active phase for Fischer-Tropsch synthesis. J Am Chem Soc 2012;134:15814–21.
[47] Wang XC, Liu L, Chen Z, et al. Large-area high-quality 2D ultrathin Mo_2C superconducting crystals. Nat Mater 2015;14:1135–41.
[48] Naguib M, Kurtoglu M, Presser V, et al. Two-dimensional nanocrystals: Two-dimensional nanocrystals produced by exfoliation of Ti_3AlC_2. Adv Mater 2011;23:4248–53.
[49] Naguib M, Mochalin VN, Barsoum MW, et al. Two-dimensional materials: 25th anniversary article: MXenes: A new family of two-dimensional materials. Adv Mater 2014;26:992–1005.
[50] Tuo MF, Xu C, Mu HR, et al. Ultrathin 2D transition metal carbides for ultrafast pulsed fiber lasers. ACS Photonics 2018;5:1808–16.